Journal of Materials Chemistry C

PAPER

View Article Online
View Journal | View Issue

Published on 11 August 2016. Downloaded by Georgia Institute of Technology on 17/10/2016 23:33:42.

Cite this: J. Mater. Chem. C, 2016, 4, 8953

# A facile and low-cost route to high-aspect-ratio microstructures on silicon *via* a judicious combination of flow-enabled self-assembly and metal-assisted chemical etching

Liyi Li, Bo Li, Chuchu Zhang, Chia-Chi Tuan, Zhiqun Lin* and Ching-Ping Wong*

A viable and low-cost strategy for fabricating high-aspect-ratio microstructures on silicon (Si) based on a judicious combination of flow-enabled self-assembly (FESA) and metal-assisted chemical etching (MaCE) is reported. First, polymer patterns were directly formed on a bare Si substrate in one step by FESA of polymers in a two-parallel-plate setup consisting of a fixed upper plate and a movable lower Si substrate that was placed on a programmable translation stage. The implementation of FESA to yield polymer patterns eliminates the complicated manipulation of polymer resist in conventional lithography methods. Subsequently, these polymer patterns were utilized as a stable etching mask in the MaCE step and exhibited a remarkable selectivity of 467 : 1 over Si during etching. Notably, such a combined FESA and MaCE strategy (*i.e.*, a FESA–MaCE route) avoids the use of a hard mask which is necessary for the conventional plasma etching method. During MaCE, a layer of Au thin film was used as a catalyst and hydrogen peroxide–hydrofluoric acid solution was employed as the etching solution. Consequently, trenches and gratings on Si at a micrometer scale with uniform controllable geometry were successfully produced. The aspect ratio of microstructures was up to 16 : 1 and the lateral edge roughness was below 0.5 μm. The influence of processing conditions on the geometry of the etched structures was scrutinized through a comparative study. The geometry of the etched structures was found to effectively adjust their surface wettability in a continuous manner. Clearly, due to the ease of implementation and the batch processing capability, the FESA–MaCE strategy is promising in manufacturing a broad range of high-quality Si-based devices at low cost.

Received 3rd May 2016,
Accepted 6th August 2016

DOI: 10.1039/c6tc01798c

www.rsc.org/MaterialsC

## 1. Introduction

Fabrication of high-aspect-ratio (HAR) microstructures on silicon (Si) is a fundamental process in manufacturing microelectromechanical systems (MEMS),[1–3] microfluidic channels,[4–6] optoelectronic devices[7,8] and components in microelectronic packaging.[9–11] The traditional strategy for producing these structures involves the use of photolithography to form patterns, followed by plasma etching to selectively remove a certain volume of Si. In photolithography, a layer of photosensitive materials, referred to as a photoresist, is coated on Si. The photoresist is then exposed to UV-visible light with the coverage of a photomask that carries designed patterns, while the patterns are transferred on the photoresist. Subsequently, the patterns in the photoresist are further transferred to a hard mask and finally to Si by two consecutive plasma-etching steps (Fig. 1(a)–(d)). This traditional route is referred to as the photolithography–plasma etching route in this paper. Photolithography has been widely used in the semiconductor industry with a resolution down to tens of nanometers.[12] Plasma etching is a traditional method to etch Si; modified versions of the plasma etch, for example, the Bosch process or cryogenic etching, are used to create HAR trenches into Si substrates with a width on a submicron scale and an aspect ratio over 100 : 1.[13,14] However, the photolithography and plasma etching incur high instrumentation and materials costs. Moreover, as most of the photoresist is heavily damaged in the plasma etching of Si, hard masks, such as $SiO_2$ or $Si_3N_4$ thin film, are necessary to protect the Si from being etched. It is not surprising that the necessity of a hard mask adds additional cost to the overall process.

In order to lower the fabrication cost of HAR microstructures, several alternative methods have emerged to potentially replace either the photolithography or plasma etching. For example, to replace photolithography, NT lithography has been used to transfer patterns on thermoplastic polymer materials *via* a stamping process.[15] Although this method is relatively cheaper

*School of Materials Science and Engineering, Georgia Institute of Technology, 771 Ferst Drive, Atlanta, GA 30332, USA. E-mail: zhiqun.lin@mse.gatech.edu, cp.wong@mse.gatech.edu*

Published on 11 August 2016. Downloaded by Georgia Institute of Technology on 17/10/2016 23:33:42.

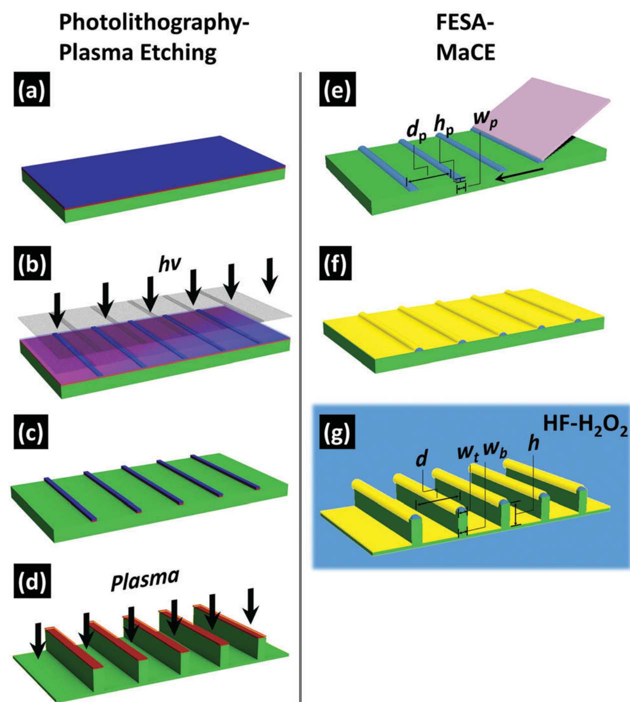


Fig. 1 Schematic illustration of the photolithography–plasma etching route and the FESA–MaCE route for HAR microstructure fabrication on Si: (a) coating of a hard mask and a photoresist; (b) photolithography; (c) geometry transfer on a hard mask; (d) plasma etching of Si; (e) FESA; (f) deposition of a metal catalyst; (g) MaCE. The blocks shown in blue, red, green, purple and golden colours refer to the photoresist/polymer, the hard mask, the Si substrate, the plate and the metal catalyst, respectively.

than photolithography by avoiding the use of UV-visible light, the instruments for thermal and mechanical treatment of the thermoplastic polymer is still expensive. On the other hand, several alternatives to plasma etching, such as the wet solution-based KOH etching[16,17] or anodic etching,[18,19] have been developed. However, their ability to fabricate uniform HAR structures with defined geometries is still limited. For example, in KOH etching, the critical dimensions of etched features are typically larger than tens of micrometers. The etching direction is dependent on the crystalline orientation of Si substrates. In anodic etching, although deep pores with diameters below one micrometer can be fabricated, their geometry generally does not follow that of the etching mask, and random branching of the pores always occurs. Therefore, the controllability of the etching profile is relatively poor.

Herein, we report a viable and low-cost strategy for crafting HAR microstructures on Si by combining the flow-enabled self-assembly (FESA) of polymers for pattern formation, with metal-assisted chemical etching (MaCE) for deep etching of Si. FESA is an effective pattern formation method which utilizes the self-assembly of polymer molecules with the guidance of the flow of the polymer solution.[20–22] The width of the polymer lines ($w_p$) and the spacing distance between the lines ($d_p$) can be facilely and precisely controlled by the time of the move and the stop step of a translation stage (Fig. 1(e)). Fabrication of uniform lines of polymers with $w_p$ and $d_p$ on a micrometer scale by FESA within several minutes has been successfully demonstrated. There are several distinctive merits of FESA compared to other available lithography technologies: (1) convenient setup and operation. Patterns are directly formed in one-step on Si, without the need for coating, curing, exposure and developing of a polymer resist as those in photolithography and electron beam lithography; (2) low cost. Only block copolymer solution and a movable stage are used, the cost of tools and materials are approximately one or two orders of magnitudes lower than that in photolithography; (3) high throughput in high volume production. Due to the simplicity of the operation, patterns can be formed at high speed. Patterns were formed over a 1 × 2 cm$^2$ area within 10 min. The throughput of the FESA technique can be increased further by accelerating the evaporation process, for example, *via* heating up the Si substrate. Similar workload may take 2–10 times longer time in electron beam lithography. If considering the time of polymer resist processing, the time of traditional lithography methods is even longer. Given these merits, FESA is potentially applicable in high-volume manufacturing of microscale patterns on Si with low cost and high throughput.

Meanwhile, we propose to use MaCE to replace plasma etching. MaCE is a wet etching method which uses a certain proportion of hydrofluoric acid (HF)–hydrogen peroxide ($H_2O_2$) mixture solution as the etchant. In experiments, Si substrates with polymer patterns are coated with a thin layer of a metal catalyst, and then immersed in HF–$H_2O_2$ for wet etching (Fig. 1(f) and (g)):[23–32]

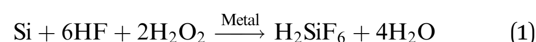

$$Si + 6HF + 2H_2O_2 \xrightarrow{\text{Metal}} H_2SiF_6 + 4H_2O \quad (1)$$

As the etching proceeds, the metal catalyst moves into Si and keeps facilitating the etching, which finally results in HAR structures in the Si substrates. Recently, by using a nanoporous catalyst and etchant solution with optimized composition, fabrication of uniform deep trenches and holes on a micrometer scale by MaCE has been demonstrated, where photolithography and electron beam lithography were used for pattern formation.[33–35] The lateral geometry of these HAR structures, such as the top width ($w_t$), bottom width ($w_b$) and spacing distance ($d$) could be accurately controlled by the lithography as well as the etching condition (Fig. 1(g)), which makes it a preferential etching method among other wet etching methods. It should be noted that previously we have discovered that only a thin layer of the polymer, either a photoresist (~1.5 µm-thick) or an electron beam resist (~200 nm-thick), was able to serve as the etching mask in MaCE. This feature enables the direct use of polymer patterns fabricated using the FESA method as an etching mask for the MaCE method, thus eliminating the need for a hard mask. It makes the proposed method not only fabrication friendly but also cost-effective. In the following sections, the fabrication of HAR microstructures using the combination of FESA and MaCE methods will be presented.

## 2. Experimental

(100)-oriented single-crystalline Si wafers (phosphorous doped, resistivity = 1–10 ohm cm) were cut into 1 × 2 cm$^2$ pieces and

 This journal is © The Royal Society of Chemistry 2016

 

Published on 11 August 2016. Downloaded by Georgia Institute of Technology on 17/10/2016 23:33:42.

washed with Piranha solution (a mixture of 96 wt% $H_2SO_4$ and 30% $H_2O_2$ with a volumetric ratio of 1 : 1) at 120 °C for 10 min before use. For FESA, parallel lines of the polymer were formed on Si wafers from a solution of poly(styrene-*block*-methylmethacrylate) in toluene with a concentration of 4 mg $mL^{-1}$. The polymer was supplied by Polymer Source (Dorval, Canada). The number average molecular weight ($M_n$) of the styrene block and the methylmethacrylate block were 135 000 and 134 000, respectively. During FESA of the polymer, the polymer solution was placed between a lower movable Si substrate and an upper slanting plate by a pipette. The upper plate was fixed while the Si substrate was carried by a computer-controlled translation stage (Parker Hannifin Corp. mode: MX80LVixBL2b). As the Si substrate was moved by the stage, the polymer solution moved together with the edge of the plate; while the stage remained stationary, due to the coffee-ring effect, the capillary flow induced by the higher evaporation rate at the drying front carried and made the polymer solutes deposited at the contact line, and thus a polymer line was formed. The resolution of the translation stage was 100 nm. The moving speed of the Si substrate was set at 2 mm $s^{-1}$ with stop times ranging from 0.1 s to 5 s to control the width of the polymer lines. The whole process mentioned above was conducted in open air in a chemistry lab at room temperature (23 °C).

After the polymer patterns were formed on Si by FESA, a cleaning process was applied on the sample using argon (Ar)/oxygen ($O_2$) plasma (referred to as the "descum" process in the following discussion) in a RIE system (Vision RIE 320, Advanced Vacuum). During the descum process, the RF power was set at 22 W and the flow rates of Ar and $O_2$ were set at 45 sccm (standard cubic centimeter per minute) and 5 sccm, respectively. The chamber pressure was set at 100 mTorr. The thickness and the morphology of the polymer lines before and after descum were characterized by an atomic force microscope (AFM, Dimension Edge, Veeco). Then a layer of gold (Au) film was deposited on the sample by an electron beam evaporation (Denton Explorer, Denton Vacuum) at a rate of 0.5 Å $s^{-1}$. The real thickness of the Au film was measured to be 14.3 ± 0.5 nm by AFM. MaCE was conducted by immersing the sample in a HF–$H_2O_2$ aqueous solution at room temperature. In the MaCE experiment with electric bias, the backside of the Si sample was coated with 10 nm Ti/100 nm Cu by electron beam evaporation and mounted on a home-made Si carrier. The bias was provided using a potentiostat (VersaSTAT, Princeton Applied Research). The details of the experiment have been reported in ref. 34. After etching, the sample was thoroughly rinsed with deionized (DI) water and dried under $N_2$ gas. The top surface and cross section of the samples after FESA–MaCE were viewed under a scanning electron microscope (SEM, Hitachi SU8010, Hitachi). For water contact angle measurements, the samples were rinsed with acetone and $KI/I_2$ aqueous solution consequently to remove the polymer and the Au. Then the samples were washed in Piranha solution at 120 °C. For silane surface treatment, the samples were immersed in a 3 mM solution of 1*H*,1*H*,2*H*,2*H*-perfluorooctyl-trichlorosilane in hexane for one hour, followed by rinsing with isopropyl alcohol and heat treatment in an atmospheric oven at 150 °C for one hour.

# 3. Results and discussion

In published literature reports, selective etching on Si could be enabled by metal patterns in HF–$H_2O_2$ after lift-off of the mask layer,[36] because the Si under the metal patterns was etched much faster than that without any metal coverage.[37] In this process, a layer of metal thin film was deposited on Si substrates with polymer (or photoresist) patterns, and then the polymer was dissolved in an organic solvent so that the metal on the polymer was removed as well. In order to retain the metal patterns on the Si surface, the metal needs to have strong enough adhesion on Si, which is typically realized by adding an adhesion layer (*e.g.* Ti or Cr) during the deposition of a metal catalyst.[38] However, in the context of this paper, in order to achieve uniform etching on a micrometer scale, nanoporous Au film is used, otherwise the Au film would easily deform randomly due to the lack of HF transport through the Au film.[33,39] The nanoporous Au film is formed spontaneously on the oxygen-terminated Si surface during the deposition of Au, without any adhesion layer in between.[40] No lift-off process should be done before etching, otherwise the Au patterns in contact with Si may be lift off as well. In other words, the polymer needs to remain between Au and Si in order to prevent the Au in contact with Si, which makes it work similar to the hard mask in plasma etching. In this sense, the polymer lines can be regarded as a mask, although MaCE is fundamentally mask-less. Based on the above argument, the stability of the polymer is indeed a crucial issue in the FESA–MaCE processing flow, which is addressed in detail in this paper.

After FESA, highly uniform polymer lines were formed on the Si surface (Fig. 2(a)). AFM was used to measure the 3D geometry of these lines. The $w_p$ and $d_p$ were measured to be 8.31 ± 0.08 μm and 22.0 ± 1.0 μm, respectively. The polymer lines showed hill-shape cross sections under AFM with steep walls (Fig. 2(b) and (f)). At the edge of the polymer lines, some polymer residue extended out into the bare Si area. Interestingly, the overall cross section of the polymer lines was slightly tilted, possibly due to the fact that the plate was slanted with respect to the Si substrate during FESA. The inclination of the fixed plate is another possible cause for the tilting of the height profile of the polymer lines.

The maximum height of the polymer lines ($h_p$) was measured as 85.7 ± 3.3 nm. All the above dimension values are the average of 5 separate measurements over the Si samples. In order to demonstrate the feasibility of using a polymer as the etch mask for MaCE, the Si sample with polymer lines was immersed in the etchant solution of MaCE, *i.e.* HF–$H_2O_2$ solution for different times. Here we defined the term $\rho$ = [HF]/([HF] + [$H_2O_2$]), where [HF] and [$H_2O_2$] stand for the concentration of HF and $H_2O_2$ in moles per liter (M). The composition of HF–$H_2O_2$ solution is expressed in the format of $\rho(x)^y$, where $x = \rho$ and $y$ = [HF]. Fig. 2(c)–(e) show the AFM

This journal is © The Royal Society of Chemistry 2016 

View Article Online



Published on 11 August 2016. Downloaded by Georgia Institute of Technology on 17/10/2016 23:33:42.

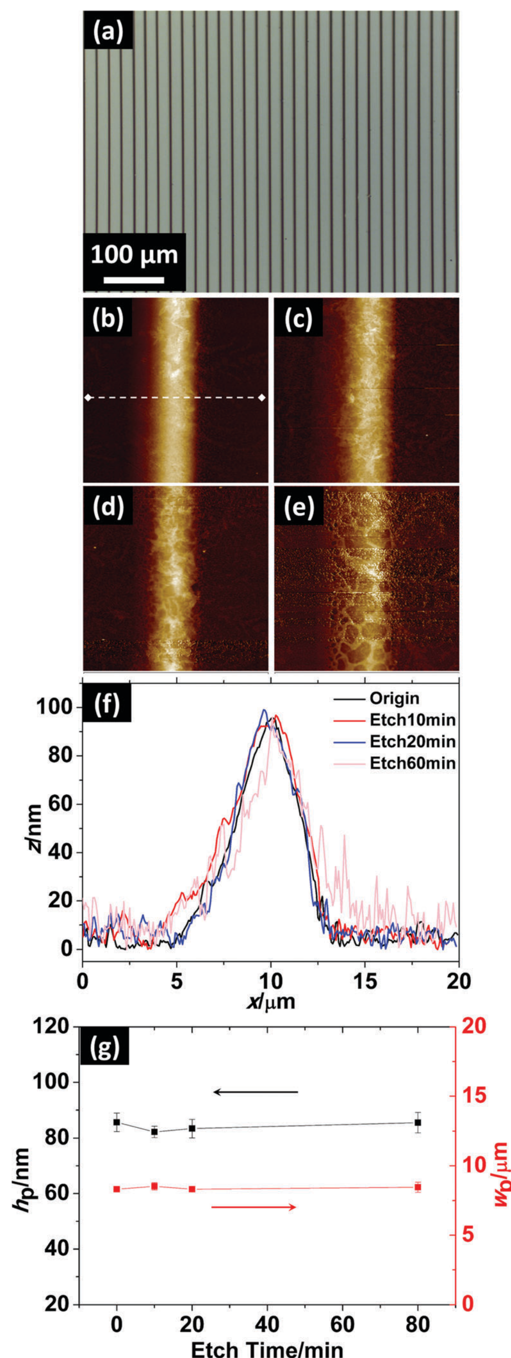


Fig. 2 (a) Optical microscopy image of the Si surface after FESA. The polymer assemblies patterned by FESA appear as the vertical black lines, while the green area in between the lines represents the bare Si surface. (b)–(e) AFM image of the polymer lines after immersion in $\rho(0.34)^{1.6}$ solution for 0 min, 10 min, 20 min and 60 min, respectively. The actual window size is 20 × 20 μm². The corresponding AFM height profiles are shown in (f), while the $h_p$ and $w_p$ measured from the AFM height profile are shown in (g).

image of the polymer lines after immersion in $\rho(0.34)^{1.6}$ solution for 10 min, 20 min and 60 min, respectively. The corresponding height profiles are shown in Fig. 2(f). Here since no metal catalyst was deposited, the etching of bare Si in the HF–$H_2O_2$ solution was negligible.[37] The $w_p$ and $h_p$ of the polymer lines are further plotted against the immersion time in Fig. 2(g). In comparison, the overall profiles of the polymer lines do not have significant variation during the immersion, although the surface roughness slightly increased in the sample after immersion for 60 min.

The stability of the polymer lines under plasma cleaning was also investigated. Here we used Ar/$O_2$ plasma to clean the trace amount of residue on the bare Si surface (the descum process) so that the metal catalyst could directly contact the Si surface and facilitate subsequent MaCE. During the plasma treatment, the size reduction of the polymer has also been observed.[41] Here for the polymer lines by FESA, we observed a similar phenomenon. As shown in Fig. 3, both $w_p$ and $h_p$ reduced with an increase in descum time. As the descum time was prolonged to 3.5 min, most of the polymer lines were cleared and the bare Si surface within the polymer lines was exposed (Fig. 3(g) and (h)). The results indicate that the size of the polymer can be further controlled by the plasma treatment after the FESA step.

After the FESA and descum steps, Au thin film was deposited on the sample and MaCE was conducted in the $\rho(0.34)^{1.6}$ etchant solution. The thickness of the Au film was controlled to 14.3 ± 0.5 nm, where nanopores existed within the Au film to facilitate uniform etching.[33] During MaCE, the overall chemical reaction shown in eqn (1) can be written in two half reactions:

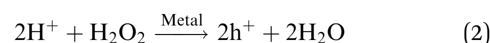

$$2H^+ + H_2O_2 \xrightarrow{\text{Metal}} 2h^+ + 2H_2O \quad (2)$$

$$Si + 6HF + 4h^+ \rightarrow H_2SiF_6 + 4H^+ \quad (3)$$

Eqn (2) describes the generation of electronic holes ($h^+$) by catalytic decomposition of $H_2O_2$ on the Au surface; eqn (3) describes the oxidative dissolution of Si with $h^+$ and HF. In the area where the Au was in direct contact with Si, the Si was etched following the above processes; in the area where Au was on the polymer lines, injection of $h^+$ from Au into Si was blocked because the polymer lines were electrically insulative, and the Au does not penetrate through the polymers. The metal catalyst does not penetrate into the Si under the polymers because: (1) the FESA patterns are not etched in the HF–$H_2O_2$ etching solution, as evident in Fig. 2; (2) the FESA patterns are solid without pores for Au to penetrate. Therefore, Si under the polymer lines remained intact during MaCE. As shown in Fig. 4(a)–(h), trenches/microgratings were formed after a MaCE time of 10 min on Si samples with different descum times. These structures possess a smooth surface and geometric uniformity in both vertical and lateral directions (Fig. 4(i) and (j)). The edge roughness, which is measured from maximum variation of the 3.2 μm-wide microgratings in Fig. 4(j), was below 0.5 μm (Fig. 4(j)). The high uniformity of the results is enabled by the excellent fabrication precision of both the FESA and MaCE steps and comparable to that of the conventional photolithography–plasma etching route.

From the results in Fig. 4(a)–(h), it is clear that the descum time significantly influences the lateral geometry, $w_t$ and $w_b$, of the etching profile by adjusting the width of polymer lines. In principle, $w_t$ and $w_b$ should exactly follow the corresponding $w_p$.

 This journal is © The Royal Society of Chemistry 2016

Published on 11 August 2016. Downloaded by Georgia Institute of Technology on 17/10/2016 23:33:42.

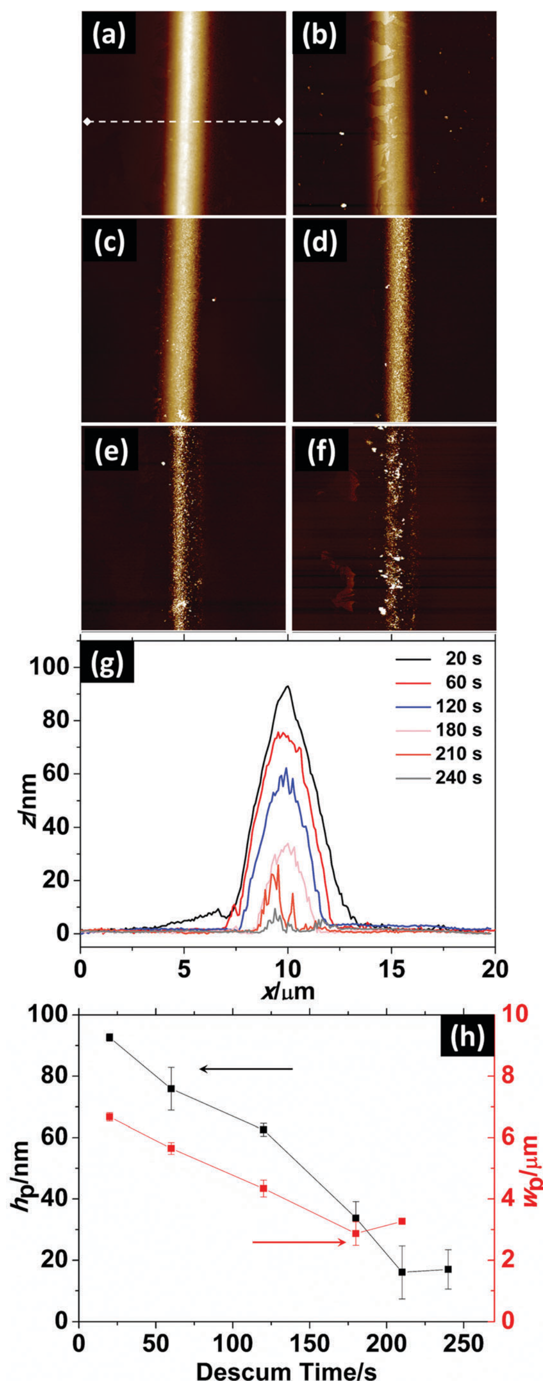


Fig. 3 (a)–(f) AFM images of polymer lines patterned by FESA on Si after descum times of 20 s, 60 s, 120 s, 180 s, 210 s and 240 s, respectively. The corresponding cross sections are shown in (g), while the corresponding $w_p$ and $h_p$ plotted against descum time in (h).

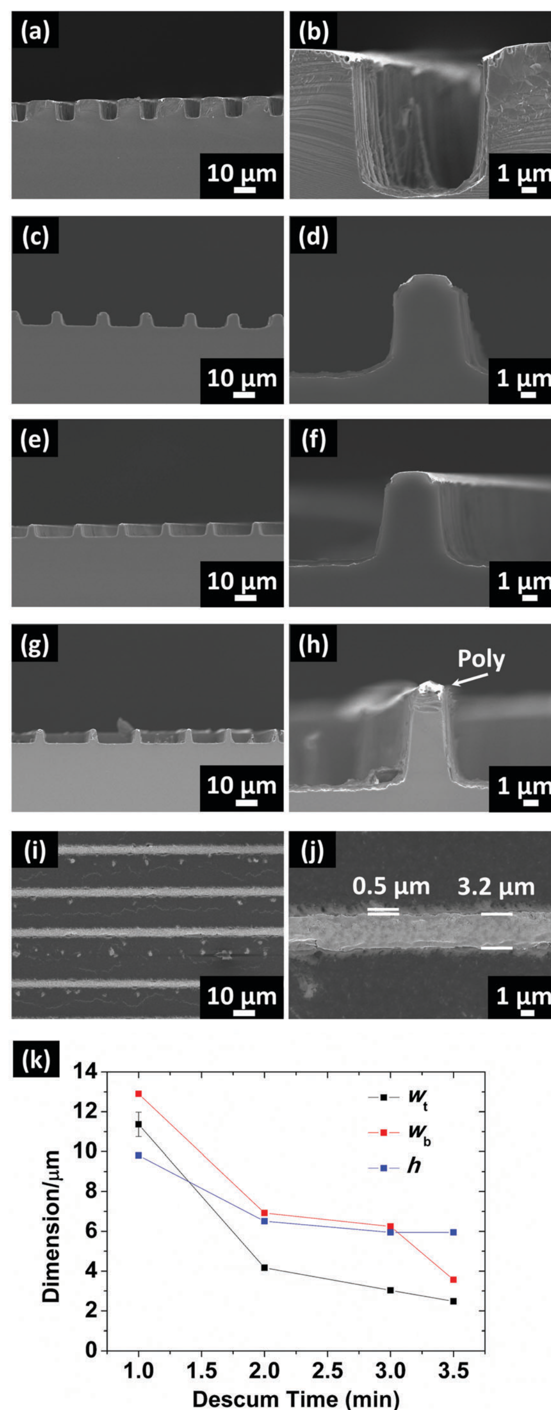


Fig. 4 Cross-sectional SEM images of the Si sample after FESA and MaCE for 10 min in $\rho(0.34)^{1.6}$ etchant solution with descum times of (a) 1 min, (c) 2 min, (e) 3 min and (g) 3.5 min. (b), (d), (f) and (h) shows the sample in (a), (c), (e) and (g) with high magnification, respectively. Top-view SEM image of the sample in (e) is shown in (i) and (j). The $w_t$, $w_b$ and $h$ of each sample are plotted against their corresponding descum times in (k). Here "Poly" refers to the polymer lines by FESA.

In experiments, when comparing Fig. 3(h) and 4(k), it can be found that $w_t$ and $w_b$ are larger than corresponding $w_p$ for the sample with a descum time of 1 min. In this case, $w_p$ was 5.6 μm, but the $w_t$ and $w_b$ were 11.3 μm and 12.9 μm, respectively. It should also be noted that for the sample with a descum time of 20 s, although the $w_p$ was measured as 6.7 μm, there was no observable etching phenomenon in the entire bare Si area. The results indicate that although most of the polymer was accumulated in the polymer lines after FESA, there remained a thin layer of polymer residue on the bare Si area as well. These polymer residues made the actual coverage of the polymer

Published on 11 August 2016. Downloaded by Georgia Institute of Technology on 17/10/2016 23:33:42.

larger than the $w_p$ that was measured by AFM, so $w_t$ and $w_b$ were generally larger than $w_p$. During the descum process, the polymer residue was gradually removed together with the polymer in the line patterns. As the descum time reached 2 min and above, the $w_t$ became very close to the corresponding $w_p$. The results suggest that a good pattern transfer fidelity can be achieved by the FESA–MaCE strategy.

Another interesting phenomenon revealed by Fig. 4(k) is that the $w_b$ is larger than $w_t$ in all samples. Actually in the SEM cross sections shown in Fig. 4(a)–(j), the sidewall of the etched trenches/microgratings is slanted rather than vertically aligned. Also, the Au film that was in contact with Si was found bending downward. This phenomenon can be explained by the half reactions shown in eqn (2) and (3). In the $\rho(0.34)^{1.6}$ etching solution, $H_2O_2$ was abundant and the amount of $h^+$ generated in eqn (2) might exceed the amount that could be consumed in eqn (3). Therefore, the excessive $h^+$ might accumulate in the Au–Si interface and a spatial distribution of $h^+$ was formed. Based on previous modeling results, $h^+$ concentration near the edge of Au film was much lower than that right under Au film, which led to a lower etching rate in this region.[33,35] As the etching proceeds, the Au edge gradually tilted upward and some Si near the edge was not etched, resulting in slanted sidewalls. Based on this, it can be inferred that the sidewall profile should be influenced by the composition of the etchant. Fig. 5(a)–(c) show the SEM cross sections of the samples after FESA–MaCE with a descum time of 3 min in etchant solution with different compositions. In the three sets of etchant solution, $[H_2O_2]$ values were held constant while [HF] values were 1.6 M, 2.3 M and 3.1 M, respectively. The $w_t$, $w_b$ and $h$ of each sample are plotted against their corresponding [HF] in Fig. 5(d). The physicochemical meaning of the composition of $HF–H_2O_2$, which is represented by the $\rho$ value in the manuscript, can be understood using eqn (2) and (3). As mentioned in the manuscript, eqn (2) describes the generation of $h^+$, while eqn (3) describes the consumption of $h^+$ and the dissolution of Si.

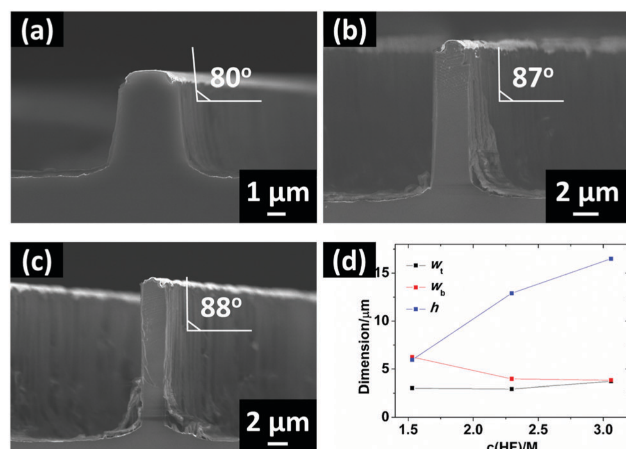


Fig. 5 Cross-sectional SEM images of the Si sample after FESA with a descum time of 3 min and MaCE for 10 min in the etchant solution with (a) $\rho(0.34)^{1.6}$, (b) $\rho(0.43)^{2.3}$ and (c) $\rho(0.50)^{3.1}$. The $w_t$, $w_b$ and $h$ of each sample are plotted against their corresponding [HF] in (d).

From the equations, it is conceivable that a higher concentration of $H_2O_2$ will render a higher amount of $h^+$, while a higher concentration of HF will make the consumption of $h^+$ faster. As $h^+$ is generated and consumed inside Si, the amount of $h^+$ at a certain moment is determined by the composition of HF and $H_2O_2$. Given the fact that $h^+$ may diffuse inside Si, the composition can be eventually correlated with the spatial distribution of $h^+$ inside Si, which determines the final etching profiles.[34] As the [HF] increased, the $h^+$ consumption rate in eqn (3) was promoted and the difference in $h^+$ concentration between the edge of Au film and its center diminished, which induced an even etching rate across the Au film. In Fig. 5(c), the sidewall angle approaches vertical and the $w_t$ is nearly identical to $w_b$, indicating a complete removal of Si near the edge of Au. The results are in accordance with the literature.[32] However, adding more HF may also increase the tendency of the breaking of the Au catalyst,[33] as some Si whiskers that protruded out of the Au film could be observed in Fig. 5(c).

To investigate the possibility of fabricating higher aspect ratios by the FESA–MaCE route, we conducted experiments with longer MaCE times. Fig. 6(a) and (b) show the cross-sectional SEM images of the samples after a MaCE time of 20 min in $\rho(0.34)^{1.6}$ etchant solution with descum times of 2 min and 3 min, respectively. $h$ in both samples increased to 14 μm. When the

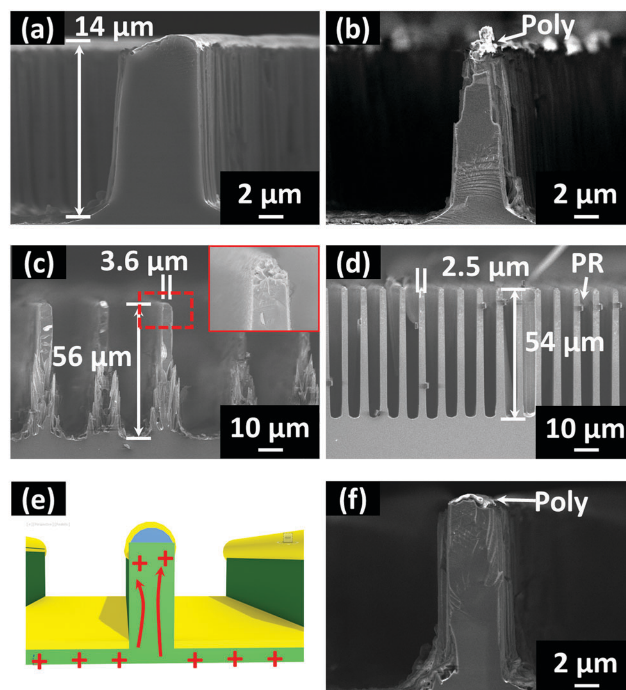


Fig. 6 Cross-sectional SEM images of the Si sample after FESA–MaCE in $\rho(0.34)^{1.6}$ with different descum times and MaCE times: (a) descum 2 min, MaCE 20 min; (b) descum 3 min, MaCE 20 min; (c) descum 3 min, MaCE 60 min. (d) Shows the results of photolithography and MaCE for 60 min. (e) Shows the schematic charge transport process during MaCE, where the blocks in green, blue and golden colours refer to Si, polymer lines and the Au catalyst, respectively. (f) Shows the results of the same experiment in (b) with the addition of −1.5 V electric bias. Here "Poly" and "PR" refer to the polymer lines and the photoresist used in FESA and photolithography, respectively.


This journal is © The Royal Society of Chemistry 2016

Published on 11 August 2016. Downloaded by Georgia Institute of Technology on 17/10/2016 23:33:42.

MaCE was prolonged to 60 min, $h$ reached 56 μm and the aspect ratio of the microgratings was 16 : 1 (Fig. 6(c)). However, a considerable amount of Si whiskers evolved at the bottom of the microgratings. We also observed that during MaCE, the polymer lines were gradually deformed (Fig. 6(b)) and finally lift off from Si (inset of Fig. 6(c)). To investigate the origin of the phenomenon, as a control experiment, we used photolithography to form the patterns and then use MaCE to fabricate the microgratings. Here a 1.5 μm-thick polymer photoresist served as the etching mask in MaCE. The microgratings made by the photolithography–MaCE strategy have similar $w_t$ and $h$, but the bottom area was uniform and no Si whiskers were observed (Fig. 6(d)). In this case, the photoresist (PR) was also observed to lift-off but retain the original shape of stripes. In comparison, because the polymer lines in FESA were only ~30 nm-thick after descum, after lift-off they broke easily and the Au on the polymer lines might etch into Si to induce the formation of Si whiskers. The consequence of the low thickness of polymer lines can also be illustrated by the etching results with a descum time of 3.5 min (Fig. 4(h)). It is clear that the polymer lines significantly deformed compared to those in Fig. 4(d) and (f). Another possible reason that causes the formation of the Si whiskers is the higher edge roughness of the FESA polymer lines compared to the photoresist patterns by photolithography. Therefore, it is possible to form HAR microgratings FESA–MaCE without Si whiskers by increasing the thickness of the polymer lines in FESA or reduce their edge roughness. The thickness and the edge roughness of the polymer lines can be adjusted by using polymers with different molecular weights or chemical functional groups, which fundamentally influence their self-assembly behavior on the Si surface.[42,43] Furthermore, we investigated the possibility of avoiding the lift-off of the polymers. As discussed above, in the $\rho(0.34)^{1.6}$ solution there may exist excessive $h^+$ in the Au–Si interfaces. These excessive $h^+$ had a chance to diffuse into the sidewall and even top of the micro-gratings so that an electrochemical etching process described in eqn (3) could occur in these regions (Fig. 6(e)).[35] Finally the Si at the top of the microgratings was removed and the polymer lines were lifted off. One way to suppress the upward diffusion of excessive $h^+$ is to apply a negative bias from the bottom of the Si sample, so the excessive $h^+$ is driven away from the top surface Si.[34] In experiments, we observed that when the same sample in Fig. 6(b) were etched with a −1.5 V negative bias, most of the damage in the top of microgratings was suppressed and the polymer lines retained their original flat profiles (Fig. 6(f)). The result supports our proposed mechanism of $h^+$ transport and the lift-off of polymer lines, and indicates that application of electric bias is an effective way to suppress the lift-off of the etching mask.

As a demonstration of potential applications, we show that the FESA–MaCE process could realize controllable surface wettability on Si samples. Recently, controlled surface wettability has found important applications in the self-cleaning surface,[44] microelectronic packaging[45] and energy harvesting.[46] It has been reported that the surface wettability can be controlled by modification of either the surface chemistry or morphology at a micro- or nanoscale. By treating the surface with low-surface

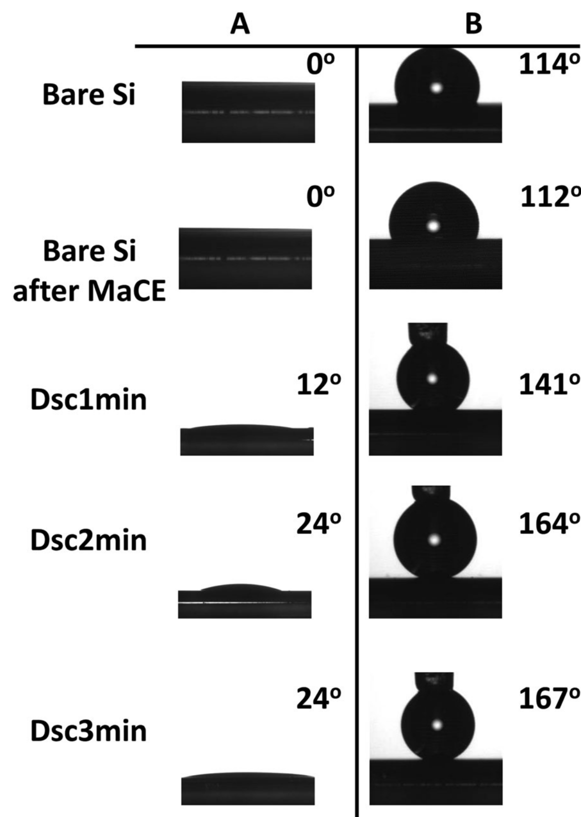


Fig. 7 Optical image of a water droplet on a bare Si surface and a Si surface after the FESA–MaCE process with different descum times. Column A shows the samples after washing in Piranha solution, while column B shows the samples after silane treatment.

energy fluoro-containing chemicals, the surface wettability is reduced and the water contact angle increases above 90°, suggesting that a hydrophobic surface is formed. Superhydrophobicity can be achieved using an additional hierarchically structured surface, and adhesion strength can be tuned by the surface structure, such as the inclined angle, pitch, and depth.[47,48] Here we quantified the surface wettability of the samples by measuring the water contact angle ($\theta$) on their surface. The samples were treated with Piranha solution and then silane solution. The bare Si surface was used as the control sample. After Piranha solution treatment, $\theta$ on the bare Si surface was 0°, while $\theta$ increased to 14° on the sample after FESA–MaCE with a descum time of 1 min, and 24° on samples with a descum time of both 2 min and 3 min. After silane treatment, $\theta$ on the bare Si surface increased to 114°, while $\theta$ further increased to 141°, 164° and 167° on the sample after FESA–MaCE with a descum time of 1 min, 2 min and 3 min, respectively. The contact angles were tested in open air, and therefore the surface may be readily contaminated by the hydrocarbon and other contamination in the air. For the hydrophilic samples treated with piranha solution, the contact angle slowly increased from ~0° to 60–70° within 1 h and stabilized overnight. For the hydrophobic samples treated with silane, the contact angle remained relatively constant at 150–160° even overnight. The different $\theta$ values on each sample can be

Published on 11 August 2016. Downloaded by Georgia Institute of Technology on 17/10/2016 23:33:42.

attributed to the fact that after MaCE, the surface bears roughness at both the microscale (trenches and microgratings) and the nanoscale (the Si whiskers) with different geometry. Also, we tested the contact angle of bare Si substrates after MaCE without the polymer lines. The whole surface of these samples was coated with Au and etched during MaCE. After MaCE and silane treatment, the surface of the samples had a contact angle of 112°, similar to that on the bare Si. The result indicates that the microstructures on the Si samples with FESA polymer lines made the major contribution to the superhydrobicity of the samples.[47] More importantly, the different $\theta$ values between Si samples with different descum times imply that the geometry of etching profiles effectively tunes the surface wettability in a continuous manner, which can be facilely controlled by the processing conditions of FESA–MaCE (Fig. 7).

## 4. Conclusion

In summary, we demonstrated the feasibility of a facile and low-cost route based on FESA and MaCE techniques to create uniform trenches and gratings with controllable width, height and spacing distance on a micrometer scale with low cost. The aspect ratio of the structures was up to 16 : 1 and the lateral edge roughness was below 0.5 μm. The polymer lines formed by FESA, even as thin as 30 nm, can serve as a stable etching mask in MaCE during which Si was etched with a depth of 14 μm, yielding a remarkable selectivity of polymer lines over Si of 467 : 1. The geometry of polymer lines can be effectively adjusted by $Ar/O_2$ plasma, and in turn the final etching profiles can be controlled during MaCE. The 3D profiles were also found to depend on the MaCE conditions, such as the composition of etchant solution and application of electric bias. Interestingly, the geometry of the resulting etching was capable of tuning the surface wettability in a continuous manner. The low-cost nature of FESA and MaCE techniques, together with their compatibility with each other, makes the FESA–MaCE route a promising manufacturing strategy for a broad range of applications where HAR trenches/ microgratings on Si play the key roles. We envision that the microstructures created by FESA–MaCE may open an avenue to judicious combining MaCE with a variety of polymer self-assembling technologies for producing HAR structures with a broader range of dimensions. For example, when integrating MaCE with the nanoscale block-copolymer self-assembly,[49,50] high-density vertical Si 2D nanosheets and nanowires may be created for advanced energy storage materials and devices.[51]

## Acknowledgements

L. L., C. T. and C. W. acknowledge the funding support from National Science Foundation (NSF CMMI 1130876). B. L., C. Z. and Z. L. gratefully acknowledge funding support from NSF (CBET-1332780).

## References

1 F. Ayazi and K. Najafi, *J. Microelectromech. Syst.*, 2001, **10**, 169.
2 F. Ayazi and K. Najafi, *J. Microelectromech. Syst.*, 2000, **9**, 288.
3 L. Jian, M. P. Brenner, J. H. Lang, A. H. Slocum, R. Struempler, in Transducers, Solid-State Sensors, Actuators and Microsystems, 12th International Conference on, 2003, vol. 1, p. 480.
4 P. Pal and K. Sato, *J. Micromech. Microeng.*, 2009, **19**, 05003.
5 C. Wu, F. Bendriaa, F. Brunelle and V. Senez, *Microelectron. Eng.*, 2011, **88**, 1878.
6 G. M. Whitesides, *Nature*, 2006, **442**, 368.
7 G. Roelkens, D. Van Thourhout and R. Baets, *Opt. Express*, 2006, **14**, 11622.
8 D. Taillaert, P. Bienstman and R. Baets, *Opt. Lett.*, 2004, **29**, 2749.
9 M. Koyanagi, T. Fukushima and T. Tanaka, *Proc. IEEE*, 2009, **97**, 49.
10 P. A. Thadesar, A. Dembla, D. Brown, M. S. Bakir, in Interconnect Technology Conference (IITC), 2013 IEEE International 2013, p. 1.
11 Y. Aibin, J. H. Lau, H. Soon Wee, A. Kumar, H. Wai Yin, L. Wen Sheng, J. Ming Ching, V. N. Sekhar, V. Kripesh, D. Pinjala, S. Chen, C. Chien-Feng, C. Chun-Chieh, C. Chi-Hsin, H. Chih-Ming and C. Chen, *IEEE Trans. Compon., Packag., Manuf. Technol.*, 2011, **1**, 1336.
12 H. H. Solak, C. David, J. Gobrecht, V. Golovkina, F. Cerrina, S. O. Kim and P. F. Nealey, *Microelectron. Eng.*, 2003, **67–68**, 56.
13 F. Marty, L. Rousseau, B. Saadany, B. Mercier, O. Francais, Y. Mita and T. Bourouina, *Microelectron. J.*, 2005, **36**, 673.
14 J. Parasuraman, A. Summanwar, F. Marty, P. Basset, D. E. Angelescu and T. Bourouina, *Microelectron. Eng.*, 2014, **113**, 35.
15 S. Y. Chou, P. R. Krauss and P. J. Renstrom, *Science*, 1996, **272**, 85.
16 E. D. Palik, V. M. Bermudez and O. J. Glembocki, *J. Electrochem. Soc.*, 1985, **132**, 871.
17 E. D. Palik, O. J. Glembocki, I. Heard, P. S. Burno and L. Tenerz, *J. Appl. Phys.*, 1991, **70**, 3291.
18 V. Lehmann and H. Föll, *J. Electrochem. Soc.*, 1990, **137**, 653.
19 M. J. J. Theunissen, *J. Electrochem. Soc.*, 1972, **119**, 351.
20 B. Li, C. Zhang, B. Jiang, W. Han and Z. Lin, *Angew. Chem., Int. Ed.*, 2015, **54**, 4250.
21 B. Li, W. Han, B. Jiang and Z. Lin, *ACS Nano*, 2014, **8**, 2936.
22 W. Han, B. Li and Z. Lin, *ACS Nano*, 2013, **7**, 6079.
23 Z. Huang, N. Geyer, P. Werner, J. de Boor and U. Gösele, *Adv. Mater.*, 2011, **23**, 285.
24 X. Li and P. W. Bohn, *Appl. Phys. Lett.*, 2000, **77**, 2572.
25 J. Kim, H. Rhu and W. Lee, *J. Mater. Chem.*, 2011, **21**, 15889.
26 S. W. Chang, V. P. Chuang, S. T. Boles and C. V. Thompson, *Adv. Funct. Mater.*, 2010, **20**, 4364.
27 F. Bai, M. Li, D. Song, H. Yu, B. Jiang and Y. Li, *Appl. Surf. Sci.*, 2013, **273**, 107.
28 C. Chartier, S. Bastide and C. Lévy-Clément, *Electrochim. Acta*, 2008, **53**, 5509.
29 N. Megouda, T. Hadjersi, G. Piret, R. Boukherroub and O. Elkechai, *Appl. Surf. Sci.*, 2009, **255**, 6210.
30 S.-C. Shiu, S.-B. Lin, S.-C. Hung and C.-F. Lin, *Appl. Surf. Sci.*, 2011, **257**, 1829.


This journal is © The Royal Society of Chemistry 2016

View Article Online


Published on 11 August 2016. Downloaded by Georgia Institute of Technology on 17/10/2016 23:33:42.


31 O. J. Hildreth, W. Lin and C. P. Wong, *ACS Nano*, 2009, **3**, 4033.
32 C.-Y. Chen, Y.-R. Liu, J.-C. Tseng and P.-Y. Hsu, *Appl. Surf. Sci.*, 2015, **333**, 152.
33 L. Li, Y. Liu, X. Zhao, Z. Lin and C.-P. Wong, *ACS Appl. Mater. Interfaces*, 2014, **6**, 575.
34 L. Li, X. Zhao and C.-P. Wong, *ACS Appl. Mater. Interfaces*, 2014, **6**, 16782.
35 L. Li, X. Zhao and C.-P. Wong, *ECS J. Solid State Sci. Technol.*, 2015, **4**, 337.
36 O. J. Hildreth, A. G. Fedorov and C. P. Wong, *ACS Nano*, 2012, **6**, 10004.
37 C. Gondek, M. Lippold, I. Röver, K. Bohmhammel and E. Kroke, *J. Phys. Chem. C*, 2014, **118**, 2044.
38 C. Chang and A. Sakdinawat, *Nat. Commun.*, 2014, **5**, 4243.
39 N. Geyer, B. Fuhrmann, Z. Huang, J. de Boor, H. S. Leipner and P. Werner, *J. Phys. Chem. C*, 2012, **116**, 13446.
40 L. Romano, M. Kagias, K. Jefimovs and M. Stampanoni, *RSC Adv.*, 2016, **6**, 16025.
41 B. Mikhael, B. Elise, M. Xavier, S. Sebastian, M. Johann and P. Laetitia, *ACS Appl. Mater. Interfaces*, 2011, **3**, 3866.
42 M. Byun, S. W. Hong, L. Zhu and Z. Lin, *Langmuir*, 2008, **24**, 3525.
43 S. W. Hong, J. Xia, M. Byun, Q. Zou and Z. Lin, *Macromolecules*, 2007, **40**, 2831.
44 D. Qi, N. Lu, H. Xu, B. Yang, C. Huang, M. Xu, L. Gao, Z. Wang and L. Chi, *Langmuir*, 2009, **25**, 7769.
45 C.-C. Tuan, Z. Lin, Y. Liu, K.-S. Moon, C.-P. Wong, in Electronic Components and Technology Conference (ECTC), 2014 IEEE 64th 2014, p. 2231.
46 Y. Liu, A. Das, S. Xu, Z. Lin, C. Xu, Z. L. Wang, A. Rohatgi and C. P. Wong, *Adv. Energy Mater.*, 2012, **2**, 47.
47 Y. Xiu, L. Zhu, D. W. Hess and C. P. Wong, *Nano Lett.*, 2007, **7**, 3388.
48 X. Gao, X. Yao and L. Jiang, *Langmuir*, 2007, **23**, 4886.
49 X. Gu, Z. Liu, I. Gunkel, S. T. Chourou, S. W. Hong, D. L. Olynick and T. P. Russell, *Adv. Mater.*, 2012, **24**, 5688.
50 C. M. Bates, M. J. Maher, D. W. Janes, C. J. Ellison and C. G. Willson, *Macromolecules*, 2013, **47**, 2.
51 W.-S. Kim, Y. Hwa, J.-H. Shin, M. Yang, H.-J. Sohn and S.-H. Hong, *Nanoscale*, 2014, **6**, 4297.